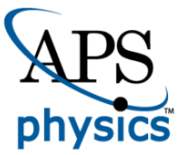

Controlling electric, magnetic, and chiral dipolar emission with PT-symmetric potentials

Hadiseh Alaeian and Jennifer A. Dionne

Phys. Rev. B **91**, 245108 — Published 5 June 2015

DOI: 10.1103/PhysRevB.91.245108

Controlling electric, magnetic, and chiral dipolar emission with PT-symmetric potentials

Hadiseh Alaeian[1,2] and Jennifer A. Dionne[2]

[1] *Department of Electrical Engineering, Stanford University, Stanford, California 94305, USA*
[2] *Department of Materials Science and Engineering, Stanford University, Stanford, California 94305, USA*

(Dated: May 13, 2015)

We investigate the effect of parity-time (PT)-symmetric optical potentials on the radiation of achiral and chiral dipole sources. Two properties unique to PT-symmetric potentials are observed. First, the dipole can be tuned to behave as a strong optical emitter or absorber based on the non-Hermiticity parameter and the dipole location. Second, exceptional points give rise to new system resonances that lead to orders-of-magnitude enhancements in the dipolar emitted or absorbed power. Utilizing these properties, we show that enantiomers of chiral dipoles near PT-symmetric metamaterials exhibit a 4.5-fold difference in their emitted power and decay rate. The results of this work could enable new atom-cavity interactions for quantum optics, as well as all-optical enantio-selective separation.

I. INTRODUCTION

The rate of spontaneous emission and the radiated power from an emitter are not intrinsic properties. Instead, an emitter's decay rate can be significantly influenced by its surroundings. Since the pioneering work of Purcell on cavity-emitter interactions [1], considerable research has explored new materials and geometries to manipulate decay rates, including photonic crystals [2–5], plasmonic structures [6–9] and metamaterials [10–13]. Each of these systems tailors light-matter interactions by modifying the local density of optical states (LDOS), which in turn dictates the number of radiative and non-radiative pathways available to an emitter for decay.

Recently, parity-time (PT) symmetric optical potentials have offered a new platform to tailor light-matter interactions. These potentials rely on the balanced inclusion of loss and gain, and render the optical Hamiltonian non-Hermitian. Below a so-called 'exceptional point', PT-symmetric systems will be characterized by a real eigenspectrum despite their non-Hermiticity [14–17]. Thereafter, eigenvalues will move into the complex plane and become complex conjugates of each other. Accordingly, optical modes can propagate preferentially in one spatial location or another, exhibiting either optical gain or strong attenuation [18–23]. The unique and unidirectional optical properties attainable with PT-symmetric potentials have enabled applications ranging from optical diodes and insulators to dual laser-coherent absorbers [24–26].

While the interaction of propagating planewaves with PT-symmetric media has been well-studied, the radiation of quantum emitters near PT-symmetric potentials remains unexplored. In this work, we investigate how PT optical potentials impact the LDOS, and, consequently, the radiation of electric and magnetic dipoles near PT-symmetric metamaterials. We begin by exploring achiral emitters, showing how both the magnitude and sign of the radiated power can be tuned. Depending on the strength of the 'non-Hermiticity parameter', the dipole can act either as a strong optical source or an efficient absorber, with positive or negative radiated powers. Further, the emitted power can be increased by several orders of magnitude at the exceptional point, where the eigenstates coalesce and increase the LDOS. Subsequently, we explore the radiation of chiral emitters near PT-symmetric metamaterials. Through appropriate design of PT-symmetric potentials, we show how enantiomers can be distinguished by their decay rate, with maximum differences observed at the exceptional point. Followed by a photoionization scheme to selectively target excited-state molecules, as proposed in [27], these results could facilitate efficient optical enantiomer separation.

II. THEORETICAL FORMULATION

We consider the planar plasmonic metamaterial shown in Fig. 1 (a), composed of a five-layer stack of alternating metallic and dielectric films. Note that this structure has recently been proposed as a PT sub-wavelength waveguide [28] and as the unit-cell constituent of a lossless, reflectionless Veselago lens [23]. As in these papers, the layers are assumed to be infinite in the xy-plane but finite in z. The metal and dielectric thicknesses, t_m and t_d, are deeply subwavelength and taken to be 30 nm. The metal is modeled as a lossless Drude material with a permittivity $\epsilon = 1 - (\frac{\omega_p}{\omega})^2$. The plasma frequency, ω_p, is taken to be $8.85 \times 10^{15} s^{-1}$, similar to bulk plasma frequency of Ag. The dielectric layers have a refractive index $n \pm i\kappa$, with one layer corresponding to loss media ($+\kappa$) and the other corresponding to gain media ($-\kappa$). For concreteness, we consider n=3.2, corresponding to the refractive index of TiO_2 in the frequency range of interest. The imaginary part of the refractive index κ is variable, but it is always identical in each dielectric layer to satisfy the PT-symmetric condition of $\epsilon(z) = \epsilon^*(-z)$. The dipole

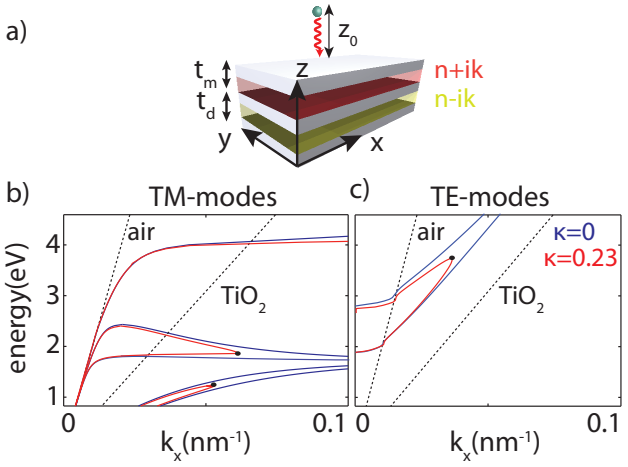

FIG. 1. (a) Schematic of a dipole radiating in the vicinity of the 5-layer PT-symmetric metamaterial. Dispersion curves of the (b) TM modes and (c) TE modes of the metamaterial for two values of the non-Hermiticity parameter, $\kappa = 0$ (blue) and $\kappa = 0.23$ (red). The black circles denote the exceptional points. The dashed lines correspond to the light lines in the air and dielectric.

emitter is assumed to be a distance z_0 away from the first vacuum/metal interface of the structure.

Fig. 1 shows the dispersion curves for the metamaterial, indicating that both transverse magnetic (TM) and transverse electric (TE) modes are supported. Each panel includes calculations for two values of the non-Hermiticity parameter, κ=0 and κ=0.23. At $\kappa = 0$, the in-plane wave vector k_x diverges for TM modes (Fig. 1 (b)) at the Ag-TiO_2 and Ag-vacuum surface plasmon resonance frequencies (E = 1.7 eV and 4 eV, respectively). Wavevectors remain finite and smaller than the TiO_2 light line for TE modes. As the non-Hermiticity parameter is increased, modes converge toward the same energy and wavevector, and coalesce at the exceptional points (EP), denoted by black circles. This point is of particular importance as it shows a phase transition in the modal behavior of the waveguide. Before this EP, the modes have real propagation constants and field distributions have a definite symmetry. After the EP however, the propagation constants move into the complex plane and the fields lose their symmetry. This region beyond the exceptional phase is called the 'broken phase.' As described in reference [28], in the broken phase, one mode is localized almost exclusively in the gain media, while the other is confined to the lossy region.

To determine how these metamaterial modes impact dipolar emission, we calculate the power radiated by a dipole, P, normalized to its radiated power in free space P_0 [29]. For an electric dipole ($\vec{p}$) the normalized radiated power of the dipole is given by:

$$\frac{P}{P_0} = 1 + \frac{3}{4}\frac{|\vec{p}_\rho|^2}{|\vec{p}|^2}\int_0^\infty Re[\frac{k_\rho}{k_z}(r_{TE} - r_{TM}k_z^2)e^{i2k_z z_0}]dk_\rho + \frac{3}{2}\frac{|p_z|^2}{|\vec{p}|^2}\int_0^\infty Re[\frac{k_\rho^3}{k_z}r_{TM}e^{i2k_z z_0}]dk_\rho \quad (1)$$

whereas for a magnetic dipole ($\vec{m}$), the radiated power is given by:

$$\frac{P}{P_0} = 1 + \frac{3}{4}\frac{|\vec{m}_\rho|^2}{|\vec{m}|^2}\int_0^\infty Re[\frac{k_\rho}{k_z}(r_{TM} - r_{TE}k_z^2)e^{i2k_z z_0}]dk_\rho + \frac{3}{2}\frac{|m_z|^2}{|\vec{m}|^2}\int_0^\infty Re[\frac{k_\rho^3}{k_z}r_{TE}e^{i2k_z z_0}]dk_\rho \quad (2)$$

In Eq. 1, $\vec{p}$, $\vec{p}_\rho$ and p_z denote the electric dipole moment and its transverse and normal components, respectively (the same for Eq. 2). Likewise, k_ρ is the transverse momentum in the xy-plane ($k_\rho = \sqrt{k_x^2 + k_y^2}$), and r_{TE} and r_{TM} are the reflection coefficients from the structure for TE- and TM-polarizations.

In general, this equation implies three important features of dipolar emission near a PT plasmonic metamaterial. First, the power strongly depends on the modal wavevector or linear momentum. Therefore, at the surface plasmon resonance frequencies where mode momenta diverge and a flat-band appears, the LDOS increases and a significant modification of the Purcell factor is expected. Secondly, the Purcell factor strongly depends on the reflection coefficient. As discussed in the next section, the reflection coefficient can be modified with increasing the non-Hermiticity parameter. An abrupt change in the behavior of the reflection coefficient at the exceptional point noticeably enhances the Purcell factor (Appendix B details the behavior of the S-matrix poles), essentially giving rise to a new system resonance. Lastly, Eq. 1 suggests that the reflection coefficient can control the sign of the power as well. As shown in Appendix A, the reflection coefficients of *evanescent* components ($k_\rho \geq k_0$) interacting with the gain or loss side of PT media are always complex conjugate of each other: $r_G = r_L^*$. For these evanescent components, k_z is purely imaginary, thus the exponential term $e^{i2k_z z_0}$ is real and the power spectrum is directly proportional to the imaginary part of the reflection coefficients. Accordingly, the non-radiative power changes sign when the reflection coefficient is replaced with its complex conjugate - or physically, when a dipole is repositioned from the loss to the gain side. Ultimately, whenever the non-radiative contribution is dominant (i.e. when the dipole is close to the structure), this feature can change the sign of the total power P. This intriguing result complements the

reports of asymmetric reflections of propagating plane waves from PT structures when illuminated from the loss of gain side [23]. In the following sections, we present the numerical results particular to the structure depicted in Fig. 1(a).

III. ACHIRAL EMITTER

Since the power emitted by a dipole is directly related to the reflected fields, we start by investigating the reflection coefficients. Figure 2(a) plots the variation of the reflection coefficient with non-Hermiticity parameter κ and in plane momentum k_ρ. We consider TM-polarized illumination, and set the energy to E=1.2eV. At this energy, all modes supported by the metamaterial lie below the vacuum light line and have real momenta exceeding that of free space (refer to Fig. 1(b)). As seen, the reflection coefficient diverges for wavevectors corresponding to the guided modes. For $\kappa = 0$, this divergence occurs for three wavevectors (k_ρ =0.006, 0.046, and 0.058 nm^{-1}). As the non-Hermiticity parameter is increased, the mode with lowest wavevector exhibits minimal variation. For better clarifications the vacuum light line is added to Fig. 2(a), as well (black dashed line). Referring to Fig. 1(b) one can clearly see that at low energies some of the TM modes closely follow the light line and only detach from the line when the energy increases. Our modal analysis for this structure (not shown here) reveals that these low momenta modes remain close to the vacuum light line even for the very large values of κ. However, the higher-momenta modes have reflection coefficients that begin to coalesce and form a loop in $k_\rho\kappa$-plane, terminating at the exceptional point, $\kappa \approx 0.23$ in Fig. 2(a). For larger values of κ, the reflection coefficient at these larger wavevectors decreases, due to the lack of momentum matching between guided modes and incident planewaves. A similar study on the reflection coefficient of TE-modes leads to a featureless map, due to the lack of TE-modes at this low energy. (see Appendix C).

Figure 2(b) shows the total power radiated by an electric dipole located 20 nm away from the metamaterial. We consider both horizontal and vertical dipoles at an energy of 1.2 eV. As seen, the Purcell factor increases by two orders of magnitude at the exceptional point. This behavior is nearly independent of dipole orientation, with slightly more power observed for the vertical dipole as it completely couples to TM modes. As seen, the behavior is very sensitive to the detuning of κ, as shown in the inset; indeed, the power rapidly decays away from the exceptional point.

Also, Fig. 2(b) indicates that the sign of the total power changes based on whether the dipole is located on the gain side (dashed lines) or loss side (solid lines) of the metamaterial. As described before, the non-radiative part of the power spectrum experiences complex conjugated reflection coefficients from the gain and loss side. This result implies that the non-radiative part of the

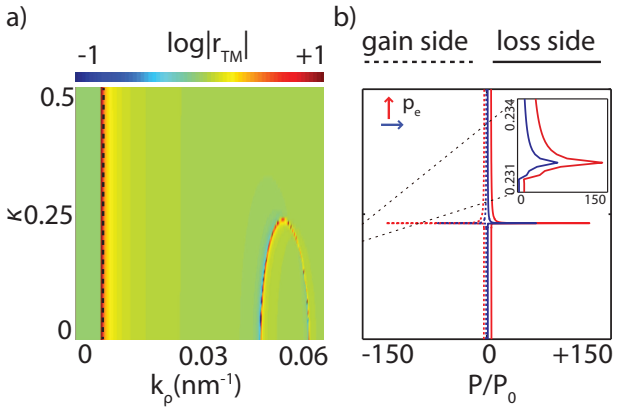

FIG. 2. (a) Reflection coefficient of TM-polarized planewave as a function of in-plane momentum and non-Hermiticity parameter κ. The energy of the planewaves is 1.2 eV. (b) Normalized power of a vertical (red lines) and horizontal (blue lines) electric dipole as a function of κ at E=1.2 eV and z_0=20 nm. The solid lines show the total emitted power when the dipole is close to the loss layer while the dashed lines correspond to the gain side. For better illustration of the behavior close to the EP the inset shows the zoomed-in version of the power normalized by the dipoles on the loss side very close to the EP. The black dotted line in panel (a) corresponds to the light line in vacuum.

power changes sign as the dipole is relocated from the gain side to the loss side. Here, the dipole's close proximity to the interface means that the non-radiative contribution dominates the radiative contribution by about two-orders of magnitude. Therefore if the sign of the non-radiative part is changed, the sign of the total power can also be changed. While the large positive power from the loss side means that the dipole behaves as an efficient emitter, the negative sign on the gain side implies that the dipole efficiently absorbs the power reflected back from the structure.

To understand this behavior further, we investigate the effect of the dual TE modes and calculate the emitted power from a magnetic dipole. Figure 3(a) plots the normalized power for both horizontal and vertical magnetic dipoles as a function of κ at a fixed energy of E=1.2eV. Here, unlike electric dipoles, the orientation of the dipoles lead to significant differences. While the horizontal magnetic dipole shows a maximum at the exceptional point ($\kappa \approx 0.23$) like the electric dipole case, the vertical magnetic dipole has no resonance feature. According to the symmetry of the radiated fields from a dipole and the modes of the structure it is clear that a horizontal magnetic dipole excites both TE and TM-polarizations while a vertical dipole exclusively couples to TE-modes. However as shown in Fig. 1(c) the structure supports no TE mode at this low energy, hence neither an EP nor a significant resonant feature will be observed at E=1.2 eV for TE-modes. Accordingly, the powers remain small for vertically-oriented dipoles. Further, note that the total power for horizontal magnetic dipoles is not symmetric.

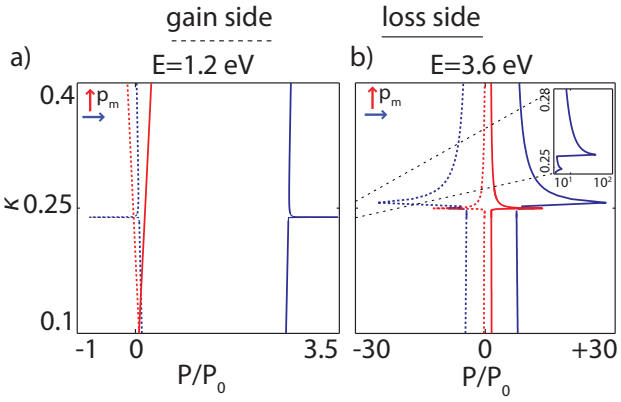

FIG. 3. Normalized power emitted by a vertical (red) and a horizontal (blue) magnetic dipole as a function of κ at (a) E=1.2 eV and (b) E=3.6 eV. The dipole is assumed to be 20 nm away from the first interface. The solid lines show the emitted power for a dipole close to the loss while the dashed lines correspond to the dipole close to the gain side. The inset in panel (b) shows the variation of the power from a horizontal magnetic dipole close to the TE-mode and TM-mode exceptional points. Note that the inset is plotted on log-scale for better clarifications.

This asymmetry is a general feature for all dipoles near PT media due to their directional scattering properties, but it is magnified for this particular case since the ratio between non-radiative and radiative contributions is small. While the non-radiative part still contributes dominantly to the total power at this short dipole-structure separation, it only is about three times larger than the radiative part.

At the energy increases, the structure supports both TM and TE modes. For example, at E=3.6 eV, the TE-reflection coefficient in the $k_\rho\kappa$-plane shows a loop at $\kappa \approx 0.25$ (see Appendix C). Therefore, unlike E=1.2 eV, at 3.6 eV both TE and TM modes have exceptional points in their spectra. Figure 3(b) shows the total power radiated by both vertical and horizontal magnetic dipoles at this energy. Unlike lower energies, resonant features in the dipole power are observed for both dipole orientations. In particular, notice that the vertical magnetic dipole, which exclusively couples to TE-modes, has a resonant peak at κ =0.25, corresponding to the exceptional point of these modes at this energy. The horizontal dipole, on the other hand, obtains two resonance features: one due to the TM-mode coalescence and another due to the TE-mode coalescence. Note that the latter coincides with the resonance features of the vertical magnetic dipole at the EP of the TE modes. For better clarification, the figure inset shows the zoomed-in version of the radiated power by a horizontal magnetic dipole in the vicinity of the TE and TM sexceptional points.

Figures 2 and 3 imply that mode coalescence at the exceptional points significantly modifies the power dissipation spectrum (the integrand of Eq. 1) and the total power. The poles of the reflection coefficients (or S-matrix) provide a deeper understanding of this phenomena. Before the exceptional point, the two simple poles, corresponding to the two slow modes below TiO_2 light line in Fig. 1(b), contribute oppositely to the integral and hence the total power. At the exceptional point, these modes coalesce and form a double pole and this opposite behavior vanishes. Therefore, a marked increase in the power is obtained. After the exceptional point, only one simple pole contributes. However the contribution of this pole monotonically decreases as the pole moves away from the real axis into the complex plane (larger κ), hence the total power decreases again. Further details can be found in Appendix B where more elaborated discussion about the singularities of the reflection coefficients and the effect of the branch-cuts and the poles are included.

The spectral variation of the radiated power as a function of energy is shown in Fig. 4. Both vertical electric and magnetic dipoles are included [30]. As seen in panels (a) and (b), which consider a dipole positioned 20 nm above the metamaterial, peaks in the normalized power appear at both frequencies of the exceptional point as well as the surface plasmon resonance frequencies. For example, a vertical electric dipole couples exclusively to TM modes and exhibits local maxima in the Purcell factor at energies of 1.2 eV and 1.9 eV (the exceptional points for the four lowest order branches) and at 2.3 eV and 4 eV. In contrast, magnetic dipole radiation cannot couple to TM modes at E=1.2 eV. However, its power spectrum has a resonance feature at E=3.8 eV, where an exceptional point arises for κ=0.23. Variation of the normalized power at lower energies is due to the appearance of the two TE modes around 1.9 and 2.7 eV.

The relative contribution of radiative and non-radiative components to the Purcell factor varies strongly as a function of z_0 (the dipole-metamaterial separation). While the non-radiative component exponentially decreases with separation, the radiative part oscillates. Since the non-radiative contribution can change the sign of the total power, the sign can in turn modified with dipole-cavity separation. Figure 4(c) plots the spatial variation of dipole power for a z-oriented electric dipole. When the dipole is close to the structure, the power is positive on the loss side and negative on the gain side. For larger separations (z$\geq$78 nm), the power radiated from the dipole is always positive, independent of its proximity to the gain or loss side. As the separation approaches infinity, the Purcell factor approaches unity, as expected. Similar trends hold for magnetic dipoles, though the magnetic dipole needs to be placed within 60 nm of the metamaterial to obtain a similar change in sign. Accordingly, a dipole located on the gain side can be tuned to behave as a bright emitter (positive power) to an efficient absorber (negative power) by changing its separation.

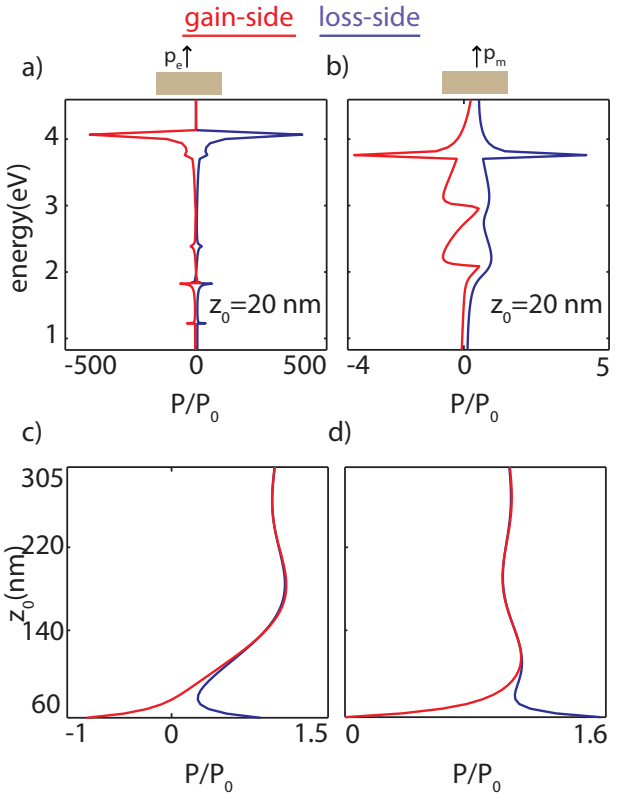

FIG. 4. Normalized power of (a) a vertical electric dipole and (b) a vertical magnetic dipole near the PT-symmetric metamaterial as a function of energy. In both cases $\kappa = 0.23$ and z_0=20 nm. The variation of the normalized power as a function of z_0 at E=4 eV and κ=0.23 is shown for (c) a vertical electric dipole and (d) a vertical magnetic dipole. Note that in these two figures the lower limit is set to z_0= 60 nm for better illustration.

IV. CHIRAL EMITTERS

While the above results pertain to electric and magnetic dipoles, the effect of the exceptional point on the radiated power is a general property of the structure and its modal features. Therefore, the results can be extended to more complicated sources, including chiral emitters. The emergence of chirality is largely attributed to the interaction of simultaneous electric and magnetic dipoles [31, 32]. Consequently, as with achiral emitters, the decay rate and radiated power of chiral molecules can be modified through its surrounding environment.

Recently, the interaction of chiral and achiral molecules with chiral objects has been the subject of extensive study [27, 33–35]. It has been shown that enantiomers exhibit enantio-specific coupling to the modes of a chiral scatterer, and that chiral structures can substantially modify the decay rate and radiation pattern of chiral molecules [27]. Here, we consider the radiation of a chiral molecule in the vicinity of our PT-symmetric structure, which, importantly, contains no chiral constituents. As will be shown, even this achiral structure can significantly modify the radiation of chiral emitters.

Equation 1 can be extended to include the simultaneous radiation of the electric and magnetic dipoles. Doing so, the normalized power radiated by a chiral source composed of an electric and magnetic dipole is given by:

$$\frac{P}{P_0} = 1 + \frac{\omega}{2P_0} Im[\vec{p}_e^{\,*} \cdot \vec{E}^s(\vec{r}_0) + \vec{p}_m^{\,*} \cdot \vec{B}^s(\vec{r}_0)] \qquad (3)$$

In this equation, $\vec{p}_e$ and $\vec{p}_m$ are the electric and magnetic dipole moments of the molecule, while $\vec{E}^s$ and $\vec{B}^s$ are the scattered electric and magnetic fields at the position of the molecule, $\vec{r}_0$. P_0 is the power radiated by a chiral source in free space. Since the magnetic moment operator is purely imaginary for a two-level system, a $\pi/2$ phase difference exists between the electric and magnetic dipoles. With this phase difference it can be shown that P_0 is given by the summation of the power emitted by each dipole in free space individually. More complex chiral molecules are characterized by a variable phase relationship and the possible need for quadrupolar terms. For simplicity, we only consider dipolar terms here. We use the common naming convention based on the sign of $\vec{p}_e \cdot \vec{p}_m$, where a right-handed enantiomer refers to a positive product, while a left-handed enantiomer refers to a negative dot product.

A schematic of a chiral molecule close to our metamaterial is shown in Fig. 5(a). The electric and magnetic dipoles are located 20 nm away from the interface, in the xy-plane with an angle θ between them. We assume that the ratio between the magnetic and electric dipoles is $\xi = 0.1c$, where c is the speed of light [27, 34]. From Fig. 3 and 4, we know achiral emitters will exhibit an increased power emission at the PT-symmetric metamaterial exceptional point. Is it possible to utilize the same LDOS enhancement at the exceptional point to manipulate the emitted power of the chiral source near PT-symmetric potentials? More importantly, do differences in the decay rates of enantiomers emerge, and can they be used to distinguish enantiomers?

For chiral selectivity, there must be an effect from the electric dipole at the position of the magnetic dipole and vice-versa. Otherwise the power radiated by each enantiomer would be the same. Since state coalescence at exceptional point manifests itself in all of the scattering parameters, an enhancement in the normalized power of the chiral emitters is expected as well. Figure 5(b) plots the difference between the normalized emitted powers (decay rates) of the right ($'+'$) and left ($'-'$) enantiomers as a function of κ. The energy again is fixed at 1.2 eV where an exceptional point appears at $\kappa \approx 0.23$. The parameters for the left enantiomer have been calculated by substituting $\vec{p}_m$ with $-\vec{p}_m$, while $\vec{p}_e$ is always fixed along the x-direction. While the difference between decay rates is minimal below the exceptional point, at this exceptional point the decay rates are markedly different. This difference monotonically increases by increasing the angle between the dipoles. Note that an x-directed elec-

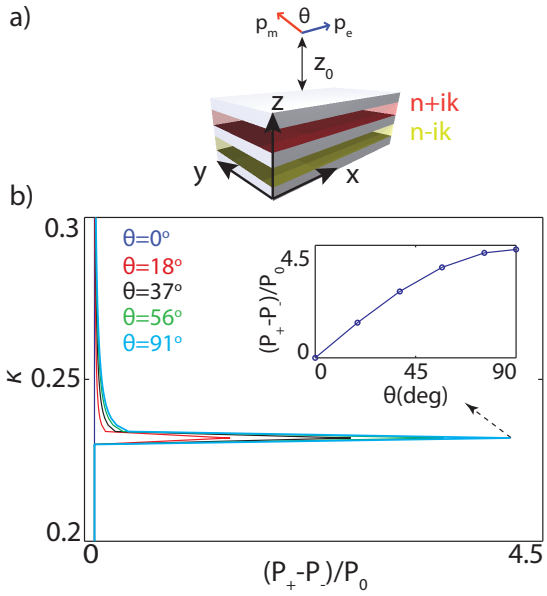

FIG. 5. (a) Schematic of a chiral molecule modelled as an electric and magnetic dipoles separated by angle θ. (b) The difference between the normalized power hence the decay rate of right (+) and left (-) enantiomers as a function of κ for different angles at E=1.2 eV. The inset shows the variation of the peak value as a function of the angle θ between the two dipoles.

tric dipole at r_0 produces only non-zero H_y at this point. Therefore, as the angle between the dipoles approaches 90^o, the scattered magnetic field by an electric dipole along the magnetic dipole increases. At $\theta \approx 90^o$, the difference between enantiomer decay rate is maximized to 4.5 [36]. In other words, if a racemic mixture of chiral enantiomers are excited, the right enantiomer decays 4.5 times faster than the left enantiomer to its ground state. Combined with a photo-ionization technique to remove molecules in the excited state, this interaction could be used to extract pure enantiomers from a racemic mixture.

V. CONCLUSION

We have studied the effect of a PT-symmetric optical potential on the radiation of achiral and chiral emitters. PT-symmetric potentials not only tune the value of the normalized power but also can change its sign. For simple electric or magnetic dipoles, mode coalescence at the exceptional point increases the emitted power by orders of magnitude. Further, PT-potentials allow for a change in the sign of the radiated power, so that a dipole can serve as a bright emitter or an efficient absorber based on its position with respect to the metamaterial (loss or gain side), and also its height above the metamaterial. Further, the exceptional point leads to a 4.5x difference in left/right enantiomer decay rates. Looking ahead, these results could be utilized in the design of new PT-symmetric cavities to control emitter properties. For example, the large Purcell factors at exceptional points could change a normally 'dark' molecule a bright emitter; or, alternatively, a bright emitter could be switched to an efficient absorber by re-locating the dipole. Such effects could be utilized in designing an efficient all-optical, single-photon modulator or a sensitive molecular ruler. The results might also pave the way for all-optical enantio-selective separation.

ACKNOWLEDGEMENTS

The authors greatly appreciate useful feedback from all Dionne group members, in particular Dr. Gururaj V. Naik, Dr. Yang Zhao and Dr. Aiztol Garcia-Etxarri. Funding from a Presidential Early Career Award administered through the Air Force Office of Scientific Research is gratefully acknowledged (FA9550-15-1-0006), as are funds from a National Science Foundation CAREER Award (DMR-1151231) and Northrop Grumman. Computational work was supported by the DOE "Light-Material Interactions in Energy Conversion" Energy Frontier Research Center under grant DE-SC0001293.

Appendix A: Scattering properties of a PT-symmetric potential

The behavior of a multilayered structure can be described using either a transfer matrix T or scattering matrix S. In our prior work, we investigated the symmetry of the scattering matrix of a PT-symmetric structure. In this appendix, we extend our analysis, describing the scattering matrix properties of PT structures excited by evanescent waves. We will show a general symmetry of $r_L = r_R^*$ relates the reflection coefficients of the structure from two sides, left (L) and right (R).

The transfer matrix favours itself to cascaded systems via the multiplication of each layer T matrix as:

$$T_{eq} = \prod_{n=1}^{n=N} T_n \tag{A1}$$

where the m^{th} layer transfer matrix is given by:

$$\begin{aligned} T_m &= [air]^{-1} I_m D_m I_m^{-1} [air] \\ I_m &= \begin{pmatrix} 1 & 1 \\ \frac{k_m}{\alpha_m} & -\frac{k_m}{\alpha_m} \end{pmatrix} \\ D_m &= \begin{pmatrix} e^{ik_m d_m} & 0 \\ 0 & e^{-ik_m d_m} \end{pmatrix} \\ [air] &= \begin{pmatrix} 1 & 1 \\ k_{air} & -k_{air} \end{pmatrix} \end{aligned} \tag{A2}$$

where $k_m = \sqrt{k_0^2 \epsilon_m - k_x^2}$ and $\alpha_m = 1$ and ϵ_m for TE and TM polarizations, respectively. From these equations the

total transfer matrix can be written as:

$$T_{eq} = [air]^{-1}(I_N D_N I_N^{-1})\cdots(I_2 D_2 I_2^{-1})(I_1 D_1 I_1^{-1})[air] \tag{A3}$$

Therefore the following equation gives the inverse of the transfer matrix as:

$$T_{eq}^{-1} = [air]^{-1}(I_1 D_1^{-1} I_1^{-1})(I_2 D_2^{-1} I_2^{-1})\cdots(I_N D_N^{-1} I_N^{-1})[air] \tag{A4}$$

if $\epsilon_m \to \epsilon_m^*$ then $I_m \to I_m^*$ and $D_m \to D_m^{*-1}$.

In a PT-symmetric potential, the permittivity distribution satisfies $\epsilon(z) = \epsilon^*(-z)$. Hence, the spatially symmetric layers either have the same real refractive indices or the permittivities are complex conjugate of each other. Assume that layer m and N-m+1 have complex conjugated permittivities. Therefore we have:

$$\begin{aligned} I_m &= I_{N-m+1}^* \\ D_m^{-1} &= D_{N-m+1}^* \\ I_m^{-1} &= I_{N-m+1}^{*-1} \end{aligned} \tag{A5}$$

hence:

$$T_m'^{-1} = T_{N-m+1}'^{*} \tag{A6}$$

where

$$T_m' = I_m D_m I_m^{-1} \tag{A7}$$

If the m^{th} layer is lossless (i.e., has a real refractive index), then k_m can be either a pure real or pure imaginary number.

case 1: k_m is real:

$$\begin{aligned} I_m &= I_m^* \\ D_m^{-1} &= D_m^* \\ I_m^{-1} &= I_m^{-1*} \end{aligned} \tag{A8}$$

hence $T_m'^{-1} = T_m'^{*}$.

case 2: k_m is imaginary:

$$\begin{aligned} T_m' &= \frac{\alpha_m}{2k_m}\begin{pmatrix} 1 & 1 \\ \frac{k_m}{\alpha_m} & -\frac{k_m}{\alpha_m}\end{pmatrix}\begin{pmatrix} e^{+ik_m d_m} & 0 \\ 0 & e^{-ik_m d_m}\end{pmatrix}\begin{pmatrix} \frac{k_m}{\alpha_m} & +1 \\ \frac{k_m}{\alpha_m} & -1\end{pmatrix} \\ &= \frac{\alpha_m}{2k_m}\begin{pmatrix} 2\frac{k_m}{\alpha_m}cos(k_m d_m) & i2sin(k_m d_m) \\ i2(\frac{k_m}{\alpha_m})^2 sin(k_m d_m) & 2\frac{k_m}{\alpha_m}cos(k_m d_m)\end{pmatrix} \end{aligned} \tag{A9}$$

Note that in this case $k_m^* = -k_m$ hence again $T_m'^{-1} = T_m'^{*}$. Now, rewrite the transfer matrix in the following form:

$$T_{eq} = [air]^{-1} A [air] \tag{A10}$$

where $A^{-1} = A^*$ and $|A| = 1$. Therefore A has the following general form:

$$A = \begin{pmatrix} a & ib \\ ic & a^*\end{pmatrix} \tag{A11}$$

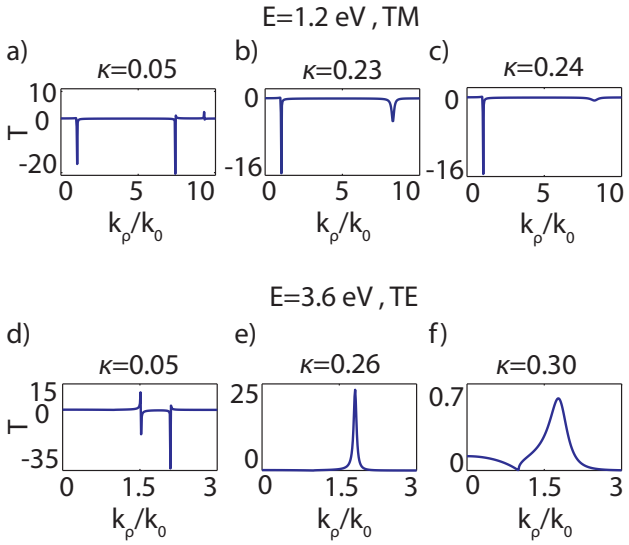

FIG. 6. Variation of the transmission coefficient as a function of in-plane momentum and various values of k for (a)-(c) TM modes at E = 1.2 eV and (d)-(f) TE modes at 3.6 eV. The non-Hermiticy values in each case are chosen to be before, at, and after the exceptional point.

Also $[air]$ is given as:

$$[air] = \begin{pmatrix} 1 & 1 \\ \sqrt{k_0^2 - k_x^2} & -\sqrt{k_0^2 - k_x^2}\end{pmatrix} \tag{A12}$$

If the waves are propagating in air, where $k_x \le k_0$ then $[air] = [air]^*$. In this case the total transfer matrix satisfies the property of $T_{eq}^* = T_{eq}^{-1}$.

However, when the waves are evanescent, i.e. $k_0 \le k_x$, this equality no longer holds. The general form for the transfer matrix is given as:

$$T = \frac{1}{2\gamma}\begin{pmatrix} 2\gamma Re(a) + (c - b\gamma^2) & +i2\gamma Im(a) + (c + b\gamma^2) \\ +i2\gamma Im(a) - (c + b\gamma^2) & 2\gamma Re(a) - (c - b\gamma^2)\end{pmatrix} \tag{A13}$$

where $\gamma = \sqrt{k_x^2 - k_0^2}$.

Although this matrix does not satisfy the previous condition of $T^* = T^{-1}$, it leads to the new equality of $r_L = r_R^*$. In other words, evanescent planewaves are reflected with complex conjugated coefficients from the gain and loss sides of a PT-symmetric potential.

Appendix B: Effect of the poles on the emitted power

In the main text, we ascribed changes in the dipolar emission near PT-symmetric potentials to the variation of the poles, hence the reflection coefficient with change of non-Hermiticity parameter. Here, we more quantitatively describe the changes of the reflection coefficients, based on the S-matrix singularities. The S-matrix singularities correspond to the modes of the system, and they

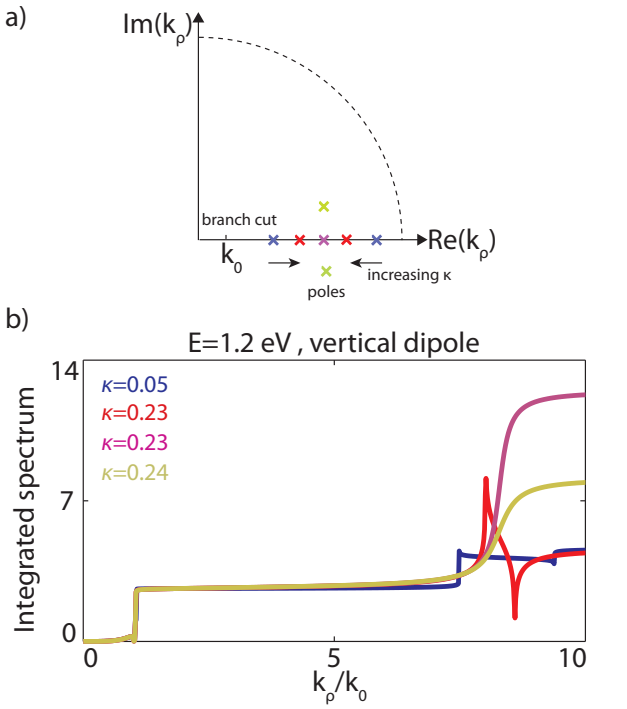

FIG. 7. (a) Location of the branch-cut and poles in k_ρ-plane (in-plane momentum) and effect of the non-Hermiticy parameter in moving the poles. (b) Partially integrated power spectrum of a vertical electric dipole at E=1.2 eV as a function of endpoint for different values of κ.

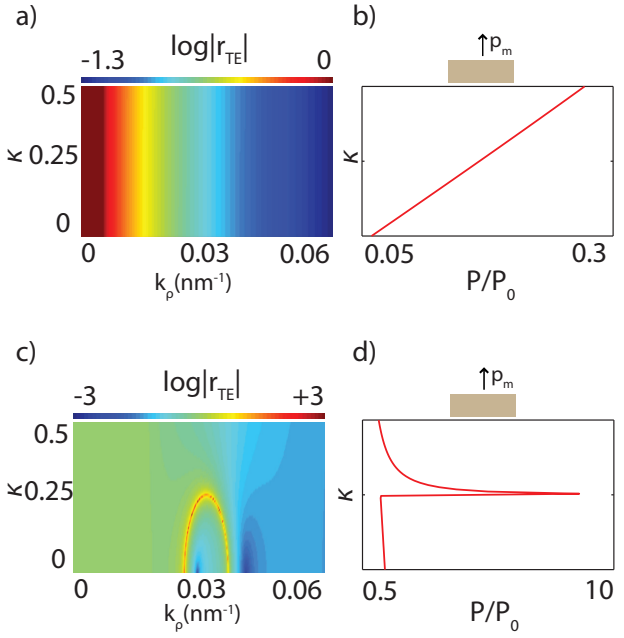

FIG. 8. Reflection coefficient of TE-mode as a function of in-plane momentum and non-Hermiticy parameter at (a) E= 1.2 eV and (c) E= 3.6 eV. Normalized power radiated by a vertical magnetic dipole located 20 nm away from the structure and on the loss side when the dipole energy E=1.2 eV(b) and E=3.6 eV(d).

appear as singularities in the reflection and transmission coefficients. As discussed before the reflection from a PT-symmetric potential is directional while the transmission is identical from both the loss and gain sides. Therefore to make the argument easier we explain the behavior based on transmission singularities and their variations with κ. Without loss of generality, a similar argument holds for the reflection coefficients as well.

Figure 6 shows the transmission coefficients of the 5-layer metamaterial as a function of k_ρ for three distinct values of non-hermiticity parameter κ. The presence of the singularities are clear from the divergence of the corresponding parameter. According to the form of the matrix elements discussed in Appendix A the type of singularities are either branch cuts (where the k_z parameters vanish) or poles (where a guided mode exists in the structure). Also the poles can only be simple since the structure is transnationally invariant hence the modes vary as $e^{i\rho k_\rho}$. Due to the loss of the layers the only branch cut occurs at $k_\rho = k_0$ as shown in Fig. 6(a)-(c). Aside from this singularity, t_{TM} shows completely different behavior for various values of κ. Referring to the dispersion diagrams of this waveguide, at E=1.2 eV the waveguide supports two deeply sub-wavelength TM-modes (modes below the TiO_2 light line in Fig. 1(a)). The wavevector of these modes corresponds to the divergence of t_{TM} in Fig. 6(a) (note the sharp resonance features in this panel at larger values). This divergence has a generic behavior of a simple pole as mentioned before, and corresponds to a non-degenerate mode in the structure. Therefore, the transmission in the vicinity of the n^{th} simple pole can be approximated as $\frac{A_n}{k_\rho - k_n}$. Note that this function changes its sign around the pole k_n. However, the different zero-crossings of the transmission close to these poles implies these residues A_n have different signs. More specifically, while the first pole has a negative to positive zero crossing the other pole has a positive to negative crossing. Therefore, the power dissipation spectrum (the integrand of Eq. 1) has simple poles with opposite residues at these points. Thus, although the structure supports two modes at E = 1.2 eV, these modes contribute oppositely to the total power of Eq. 1.

As κ increases, the poles corresponding to the modes of the structure approach each other and finally coalesce at $\kappa = 0.23$, as seen in Fig. 6(b). Notice that there is no sign change around this pole and the value is exclusively negative, a signature of a second order mode and state coalesce. Accordingly, the power dissipation spectrum around this pole can be approximated as $\frac{A'_n}{(k_\rho - k_n)^2}$. Increasing κ beyond this point leads to a significant decrease in the transmission due to the new location of the poles in the complex plane, away from the real axis. A similar behavior for the TE polarized modes at E=3.6 eV has been shown in Fig. 6 where a comparison before, at, and after the exceptional point is given in panels (d),(e)

and (f), respectively. Again, note how the two sharp resonance features accompanied by a sign change for simple poles in Fig. 6(d) is substituted with a single-valued single peak at the exceptional point in Fig. 6(e). Also note that the peak drastically decreases in Fig. 6(f) where the poles have imaginary values after the exceptional point.

To numerically validate this behavior, Fig. 7 shows the partial integral of the power dissipation spectrum, where the upper limit of the integral in Eq. 1 is replaced with a variable k_ρ. The power dissipation integral is for a vertical electric dipole radiating at E=1.2 eV. Figure 7(a) shows the contour integral path in the complex k_ρ-plane in black dashed lines. In this plane, the singularities of the integrand are denoted as branch cuts at k_0 followed by a series of poles. The black arrows schematically show the trajectory of the poles along the real k_ρ-axis when κ changes. From residue theorem, it is well-known that the integral value is given by the residue of the poles surrounded by the contour. When κ is small, corresponding to two real and distinct modes (red crosses in Fig. 7(a)), the value of the integral changes in opposite directions as the upper limit passes the poles. The residue of the integrand has different signs for these two poles. However, when κ hits the exceptional point (purple cross in Fig. 7(a)), the value of the integral monotonically increases even after passing the pole. Entering the broken phase by increasing κ (yellow crosses in Fig. 7(a)), the increasing behavior could be preserved, but the integral values are substantially smaller. Since in this regime the poles move away from the real axis, the contribution from these poles decrease the integral values in the limit of $\kappa_\rho \to \infty$. This quantitative assessment agrees with the qualitative behavior of the poles deduced from the scattering parameters. More importantly, it reveals the underlying effect of the exceptional points on dipolar emission.

Appendix C: Variation of reflection coefficients for TE-modes

In the main text, the reflection coefficient of the TM modes was presented at 1.2 eV. There, it was shown that substantial enhancement in the power corresponds to the emerging exceptional point. Here, we expand upon the behavior of the magnetic dipole results presented in Fig. 3. Figure 8(a) shows the reflection coefficient of TE modes in $k_\rho\kappa$-plane at E=1.2 eV. As described in the main text, the map is nearly featureless, since there are no TE modes at this energy. Accordingly, the power of the vertical magnetic dipole is very small (Fig. 8(b)). However, the structure supports TE modes at higher energies. Figure 8(c) shows the reflection coefficient of TE modes at E=3.6 eV in the $k_\rho\kappa$-plane. In contrast to the low energy case, here a similar looping behavior occurs at $\kappa \approx 0.25$, corresponding to an exceptional point for TE modes at this energy and this non-Hermiticity factor. Since a vertical magnetic dipole exclusively excites TE modes, it is a good check to investigate the change of its power as a function of κ. Figure 8(d) shows the emitted power from a vertical magnetic dipole at E=3.6 eV. As can be seen, the normalized power increases by one order of magnitude where the corresponding exceptional point is observed in the reflection coefficient of Fig. 8(c).

[1] E. M. Purcell, Physical Review **69**, 681 (1946).
[2] S. Noda, M. Fujita, and T. Asano, Nature Photonics **1**, 449 (2007).
[3] H. Iwase, D. Englund, and J. Vukovi, Optics Express **18**, 16546 (2010).
[4] J. Canet-Ferrer, L. J. Martnez, I. Prieto, B. Aln, G. Muoz-Matutano, D. Fuster, Y. Gonzlez, M. L. Dotor, L. Gonzlez, P. A. Postigo, and J. P. Martnez-Pastor, Optics Express **20**, 7901 (2012).
[5] J. Canet-Ferrer, I. Prieto, G. Muoz-Matutano, L. J. Martnez, L. E. Muoz-Camuniez, J. M. Llorens, D. Fuster, B. Aln, Y. Gonzlez, L. Gonzlez, P. A. Postigo, and J. P. Martnez-Pastor, Applied Physics Letters **102**, 201105 (2013).
[6] A. F. Koenderink, Optics Letters **35**, 4208 (2010).
[7] R.-M. Ma, R. F. Oulton, V. J. Sorger, G. Bartal, and X. Zhang, Nature Materials **10**, 1101 (2011).
[8] T. V. Shubina, A. A. Toropov, V. N. Jmerik, D. I. Kuritsyn, L. V. Gavrilenko, Z. F. Krasilnik, T. Araki, Y. Nanishi, B. Gil, A. O. Govorov, and S. V. Ivanov, Physical Review B **82**, 073304 (2010).
[9] E. J. R. Vesseur, F. J. G. de Abajo, and A. Polman, Physical Review B **82**, 165419 (2010).
[10] Z. Jacob, I. I. Smolyaninov, and E. E. Narimanov, Applied Physics Letter **100**, 181105 (2012).
[11] A. N. Poddubny, P. A. Belov, and Y. S. Kivshar, Physical Review A **84**, 023807 (2011).
[12] A. N. Poddubny, P. A. Belov, and Y. S. Kivshar, Physical Review B **87**, 035136 (2013).
[13] A. Poddubny, I. Iorsh, P. Belov, and Y. Kivshar, Nature Photonics **7**, 948 (2013).
[14] C. M. Bender and S. Boettcher, Phys. Rev. Lett. , 5243 (1998).
[15] H. F. J. C. M. Bender, D. C. Brody, Physical Review Letters **93**, 251601 (2004).
[16] J.-H. C. C. M. Bender, S. F. Brandt and Q. Wang, Physical Review D **71**, 065010 (2005).
[17] C. M. Bender, Contemp. Phys. **46**, 277 (2005).
[18] D. N. C. R. El-Ganainy, K. G. Makris and Z. H. Musslimani, Optics Letters **32**, 2632 (2007).
[19] D. D. R. M. M. V.-R. V. A. G. A. S. A. Guo, G. J. Salamo and D. N. Christodoulides, Physical Review Letters **103**, 093902 (2009).
[20] D. N. C. K. G. Makris, R. El-Ganainy and Z. H. Musslimani, Physical Review Letters **100**, 103904 (2008).
[21] D. N. C. K. G. Makris, R. El-Ganainy and Z. H. Musslimani, Physical Review A , 063807 (2010).

[22] R. E.-G. D. N. C. M. S. C. E. Rter, K. G. Makris and D. Kip, Nature Physics **6**, 192 (2010).
[23] H. Alaeian and J. A. Dionne, Physical Review A **89**, 033829 (2014).
[24] Y. D. Chong, L. Ge, and A. D. Stone, Physical Review Letters **106**, 093902 (2011).
[25] X. Liu, S. D. Gupta, and G. S. Agarwal, Physical Review A **84**, 013824 (2014).
[26] S. Longhi and L. Feng, Optice Letters **39**, 5026 (2014).
[27] V. V. Klimov, D. V. Guzatov, and M. Ducloy, Europhysics Letters **97** (2012).
[28] H. Alaeian and J. Dionne, Physical review B **89**, 075136 (2014).
[29] L. Novotny and B. Hecht, *Principles of nano-optics*, 2nd ed. (Cambridge University Press, 2006).
[30] Here we only present the results for the vertical electric and magnetic dipoles since they exclusively couple to TM and TE-modes, respectively. However, a similar argument holds for the horizontal orientations with coupling to both types of modes.
[31] L. D. Barron, *Molecular Light Scattering and Optical Activity* (Cambridge: Cambridge University Press, 1982).
[32] V. Klimov and M. Ducloy, Physical Review A **72**, 043809 (2005).
[33] A. Lakhtakia, V. K. Varadan, and V. V. Varadan, J. Phys. D: Appl. Phys **23**, 481 (1990).
[34] V. Klimov, I. Zabkov, A. Pavlov, and D. Guzatov, Optics Express **22**, 18564 (2014).
[35] D. V. Guzatov and V. V. Klimov, New Journal of Physics **14**, 123009 (2012).
[36] Note that the molecular chirality vanishes at $\theta = 90^o$, therefore we present the results for $\theta = 91^o$.